Original scientific paper

Received: May 27, 2017
Accepted: Apr 09, 2018
DOI: 10.2478/rmzmag-2018-0020

High resolution airborne radiometric and magnetic studies of ilesha and its environs, southwestern Nigeria

Visokoločljivostna aeroradiometrična in aeromagnetna raziskava območja ilesha in okolice v jugozahodni nigeriji

Okeyode I. C.[1], Olurin O. T.*[,1], Ganiyu S. A. and Olowofela J. A.[1]

[1] Department of Physics, Federal University of Agriculture, P. M. B. 2240, Abeokuta Ogun State Nigeria

* stolurin@yahoo.com

Abstract

The study of the nature of distribution of natural radioelements in Ilesha and its environs with its geological structure has been studied using aeroradiometric data. Aeromagnetic data have also been subjected to three automated gradient techniques to delineate the subsurface structure of the study area. From the study, it can be found that maximum values of "eU" (ppm) and "eTh" (ppm) fall within the branded gneiss, whereas the maximum value of K (%) falls within porphyritic granite regions. eTh had the highest radioactive content. The environmental dose rate of Ilesha was between 0.1817 and 3.9296 msv/yr. Although there were extreme values, but the mean dose rate was 0.522 ± 0.310 msv/yr (within acceptable safe limit of 1.0 msv/yr). eU/K, eU/eTh and eTh/K ratios were analysed for enrichment or depletion of radioisotopes. eU/eTh >1 showed uranium depletion, while eTh >2 showed eTh enrichment. The magnetic intensity values ranged from -79.41 to 140.93 nT. The horizontal gradient method (HGM) and analytic signal amplitude (ASA) revealed that depth to magnetic sources ranged from 0.478 to 4.112 km and 0.348 to 2.551 km, respectively, whereas local wavenumber (LWN) depth ranged from 0.478 to 5.48 km, which overestimated those compared using HGM and ASA functions. The apparent susceptibility ranged from -0.00325 to 0.00323 SI, showing that ferromagnetic and diamagnetic mineral ranges control apparent susceptibility in Ilesha.

Key words: Aeromagnetic data, Apparent Susceptibility, Background Radiation Doses, Ilesha, Radiometric Data

Povzetek

Lastnosti porazdelitve naravnih radioaktivnih prvin in geološko zgradbo na območju Ilesha in okolice so proučevali z aeroradiometričnimi podatki. Za raziskavo globinske geološke zgradbe proučevnega ozemlja so uporabili tudi aeromagnetne meritve po treh avtomatskih gradientnih metodah. Iz študije sledi, da izkazujejo najvišje vrednosti "eU" (ppm) in "eTh" (ppm) območja izdankov gnajsa, največje vrednosti K (%) pa območja porfiritnega granita. Najvišje so vrednosti radioaktivnega eTh. Radioaktivna doza ozadja v Ileshiu se giblje med 0,1817 in 3,9296 mSv/a. Nastopajo ekstremne vrednosti, toda povprečna doza ozadja znaša 0,522 ± 0,310 mSv/a (znotraj sprejemljive meje 1,0 mSv/a). Z analizo razmerij eU/K, eU/eTh in eTh/K so ugotavljali obogatitve ali osiromašenja radioaktivnih izotopov; vrednost eU/eTh >1 nakazuje osiromašenje z uranom, eTh, ki je večja od 2, pa obogatitev z eTh. Vrednosti magnetne intenzitete se gibljejo med -79,1 in – 140.93 nT. Metodi horizontalnega gradienta (HGM) in amplitude analitskega signala (ASA) nakazujeta globine do virov magnetizma v razponih 0,478–4,112 km in ustrezno 0,348–2,551 km, medtem ko je razpon globin z metodo Local Wavenumber (LWN) od 0,478 do 5.48 km, kar je precenjeno glede na rezultate HGM in ASA. Navidezna susceptibilnost se giblje v razponu od -0.00325 do – 0.00323 SI, kar kaže, da je susceptibilnost v Ileshu odvisna od feromagnetnih in diamagnetnih mineralov.

Ključne besede: aeromagnetni podatki, navidezna susceptibilnost, radiacijske doze ozadja, Ilesha, radiometrični podatki

Introduction

Since the time radioactivity has been discovered, more efforts have been put into the study of the environmental natural radiation [1]. Calculations of equivalent doses from natural environments have recently been possible through ground and airborne gamma-ray surveys [2–4]. Air-borne gamma ray spectrometry measures natural emission of gamma radiation from the surface of the earth. Thorium-232 and uranium-238 decay series as well as potassium-40 are the natural radionuclides that are used for estimating the abundance of thorium, uranium and potassium in airborne radiometric surveys. Having the image of gamma rays emanating from the surface of the earth is as good as having the surface geochemical map that shows how radionuclides in rocks, soil, etc. spread [5]. Airborne geophysical survey has been a very useful tool available to Earth scientists in interpreting geology of difficult terrain [6]. The broad view of the Earth that the airborne geophysics perspective provides has been well recognised since the early days of balloon photography and military reconnaissance [7]. Aeromagnetic survey has proved essential in displaying the spatial distribution and relative abundance of magnetic minerals and nonmagnetic minerals in the upper levels of the crust, which can help in the visualisation of the geology and geological structures of the upper crust of the earth [6]. The aim of this study was to use high-resolution airborne radiometric data of Ilesha to assess and quantify naturally occurring radioactive materials in order to estimate background radiological doses of the area and correlate the data with the geological map of the area to show the distribution of the radioelements with geology. In addition, the aim of this study was to use aeromagnetic data to estimate source parameters (source location, depth and apparent magnetic susceptibility contrast) from the grid in conjunction with the local geomagnetic field parameters associated with the area under consideration using automated magnetic gradient techniques in accordance with [8].

Description and Geology of the Study Area

Ilesha is a popular town in Osun State, south western Nigeria. This city serves as a major linked way to the northern, southern and eastern parts of Nigeria. The area has remarkable agricultural potentials with production of major food crops, which include but are not limited to oil palm, cocoa, pumpkin, cotton and cola nut. Different minerals and most especially gold in commercial quantities are also available. Gold mining is one of the occupations of some artisans in Ilesha and its environs. This kind of activity has been identified with high concentrations of uranium [9]. The study cover area located between latitude 7°30´N to 8°00´N and longitude 4°30´E to 5°00´E. Ilesha and its environs lie within the basement complex (schist belt) of southwest Nigeria, which is of Precambrian age [10,11]. In 1947 and 1957, [12] and [13], respectively, suggested that the Nigerian basement complex is polycyclic. This was confirmed by Hurley [14] who used radiometric method to determine the age of the rocks. The uniqueness of this terrain is evident by complex coexistences of basement and sedimentary rock, and the contact between the two rock types is often poorly defined. The basement complex rocks of Pre-Cambrian age are made up of older and younger granites, with the younger and older sedimentary rocks (formation) of both tertiary and secondary ages. The formation is pre-drift sequence of continental sands, grits and silts (Figure 1).

In terms of structural features, lithology and mineralisation, the schist belts of Nigeria show considerable similarities to the Achaean greenstone belts. However, the latter usually contain much larger proportions of mafic and ultramafic bodies and assemblages of lower metamorphic grade [11,15]. Rocks in this area are structurally divided into two main segments by two major fracture zones often called the Iwaraja faults in the eastern part and the Ifewara faults in the western part [16,17]. The western part of the fault comprises mostly amphibolites, amphiboles schists, metaultramafites and metapelites. Extensive psammitic units with minor metapelites constitute the eastern segment. These are found as quartzites and quartz schists. All these assemblages are associated with migmatitic gneisses and are cut by a variety of granitic bodies [11]. The rocks of Ilesha district is broadly grouped into gneiss–migmatite complex, mafic–ultramafic suite (or

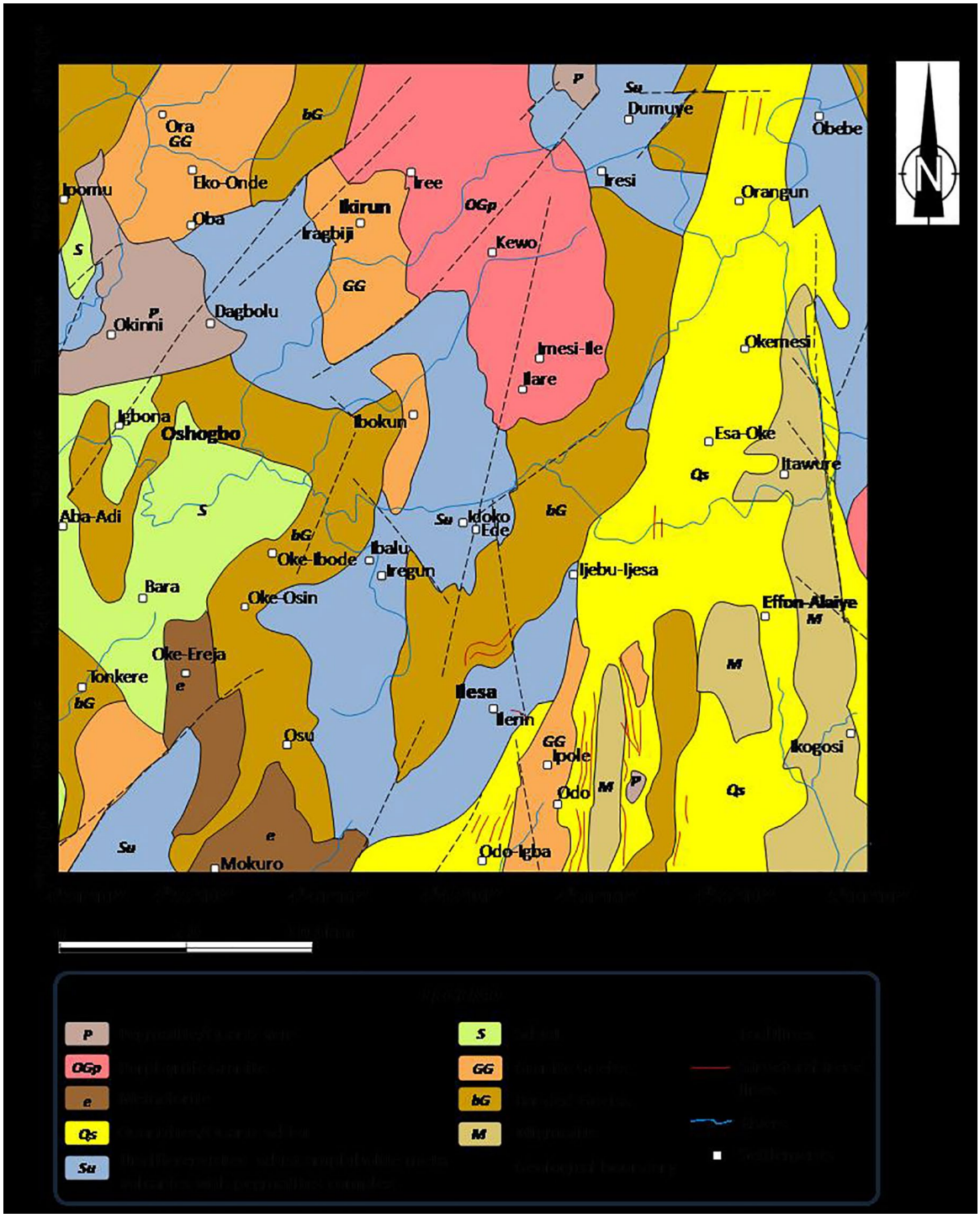

Figure 1: *Geological map of Ilesha and its environs.*

amphibolite complex), meta-sedimentary assemblages and intrusive suite of granitic rocks. A variety of minor rock types are also related to these units. The gneiss–migmatite complex comprises migmatitic and granitic, calcareous and granulitic rocks. The mafic–ultramafic suite is mainly composed of amphibolites, amphibole schists and minor meta-ultramafites made up of anthophyllite–tremolite–chlorite and talc schists. The meta-sedimentary assemblages,

chiefly metapelites and psammitic units, are found as quartzites and quartz schists. The intrusive suite consists essentially of Pan-African granitic units. The minor rocks include garnet–quartz–chlorite bodies, biotite–garnet rock, syenitic bodies and dolerites [11,16,18].

Instrumentation and Data Collection

The airborne radiospectrometric and magnetic data of Ilesha sheet number 243 on scale 1:50,000 were surveyed by the Nigerian Geological Survey Agency in 2009. The airborne potential field data were acquired at a mean altitude of 80 m with flight line separation of 400 m along the northwest–southeast direction. The aircraft travelled at the airspeed between 150 and 250 km/h, which covered the entire area under consideration. The flight line direction was in the direction 135° azimuths, while the tie line direction was in 45°. The average magnetic inclination and declination across the survey were -9.67° and -2.52°, respectively. The geomagnetic gradient was removed from the data using International Geomagnetic Reference Field (IGRF) of Epoch 2009. The flight path was generally followed by the pilot of the aircraft using a real-time differential Global Positioning System, which was also used to recover the positions of each measurement and allow the precise and accurate positioning of the survey data and integration with other spatial data. These data had been prepared for subsequent processing by digitising the maps in a numeric format that permits the application of interpolation (gridding) technique. Therefore, they had been subjected to different techniques of processing [19].

Airborne Radiometric Analysis

The distributions of the three natural radionuclides (equivalent concentrations of thorium (*eTh*), equivalent concentrations of uranium (*eU*) and equivalent concentrations of potassium (K)) present in the study area have been obtained using the surveyed radiometric data (Figures 2–4, respectively). When weathering occurs, it modifies the distribution and the concentrations of radioelements when compared to the original bedrock [20]. These gamma rays emitted from the surface are related to the weathered materials and geochemistry as well as the mineralogy of the bedrock. The plots of the radioelement ratios (eU/K, eU/Th and eTh/K) are shown in Figures 5–7, respectively. The composite image of the radioelements combines all the three data, K (%), eU and eTh, as shown in Figure 11. In order to verify the environmental effects due to these natural radionuclides, the exposure rates, E ($\mu R/hr$), and the equivalent dose rates, D(mSv/yr), were calculated using the following equations, respectively [19–22]:

$$E\ (\mu R/hr) = 1.505\ \text{K}\ (\%) + 0.287\text{eTh}\ (\text{ppm}) + 0.653\ \text{eU}\ (\text{ppm}) \quad (1)$$

$$D(mSv/yr) = 0.0833 \quad (2)$$

where eTh, eU and K are the equivalent concentrations of thorium, uranium and potassium in part per million and K (%) is potassium in percentage. The plot of the environmental radioactivity dose rates is presented in Figure 9. In order to assess the trend of uranium migration in the study area, uranium migration index was calculated using Equation (3) as stated by [19] and [23] and is plotted in Figure 10.

$$eU - \frac{eTh}{3.5} \quad (3)$$

The radiometric data have been statistically treated, and the results are summarised in Table 1.

Qualitative interpretation of airborne radiometric data

The thorium equivalent concentration contour map

The study area is enriched with some level of thorium radioactivity, most especially the northern through the southern central parts. In Figure 2, these levels can be seen to be from 0.11 to 5.22 (ppm), characterised by pegmatite/schist geological formation, 5.22–9.14 ppm, and quartzite/quartz schist geological formation, 9.14–18.59 ppm Undifferentiated schist amphibolite meta volcanic with pegmatite complex and 18.59–76.49 (ppm) characterised by Branded Gneiss. There is a high anomaly in this last range. The average value was found to

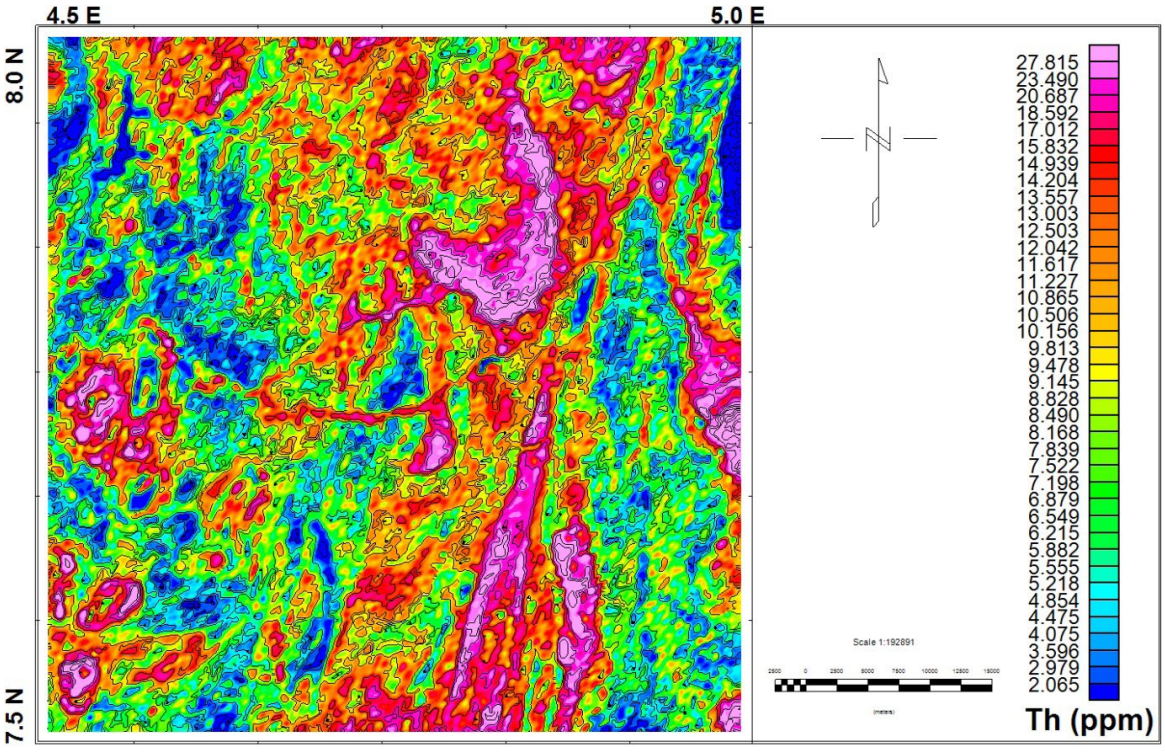

Figure 2: *Airborne radiometric thorium anomalies of the study area.*

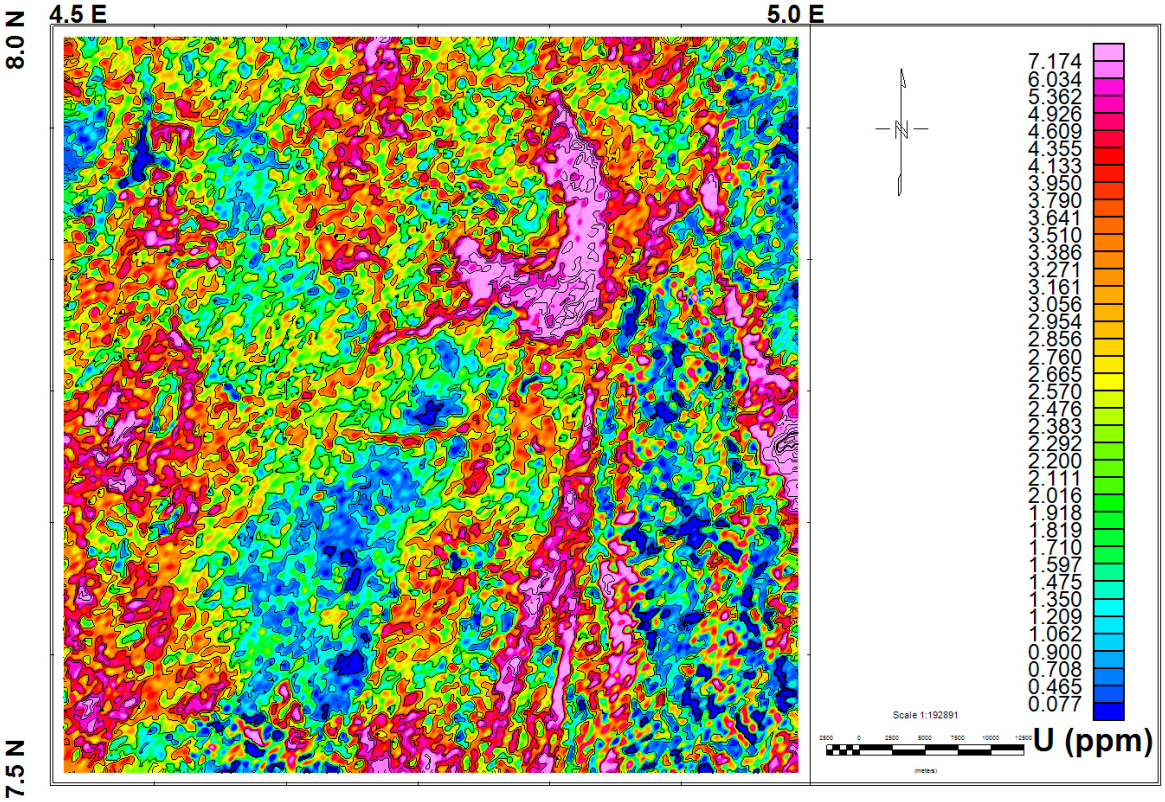

Figure 3: *Airborne radiometric uranium anomalies of the study area.*

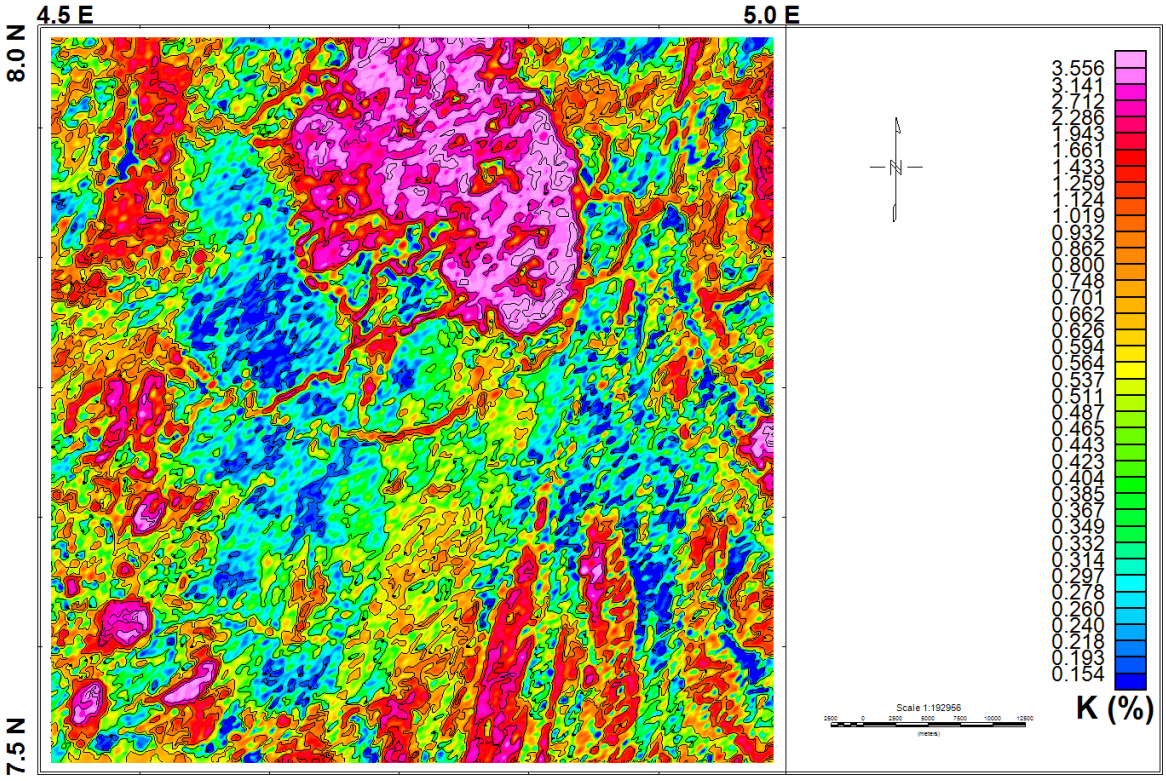

Figure 4: *Airborne radiometric potassium anomalies of the study area.*

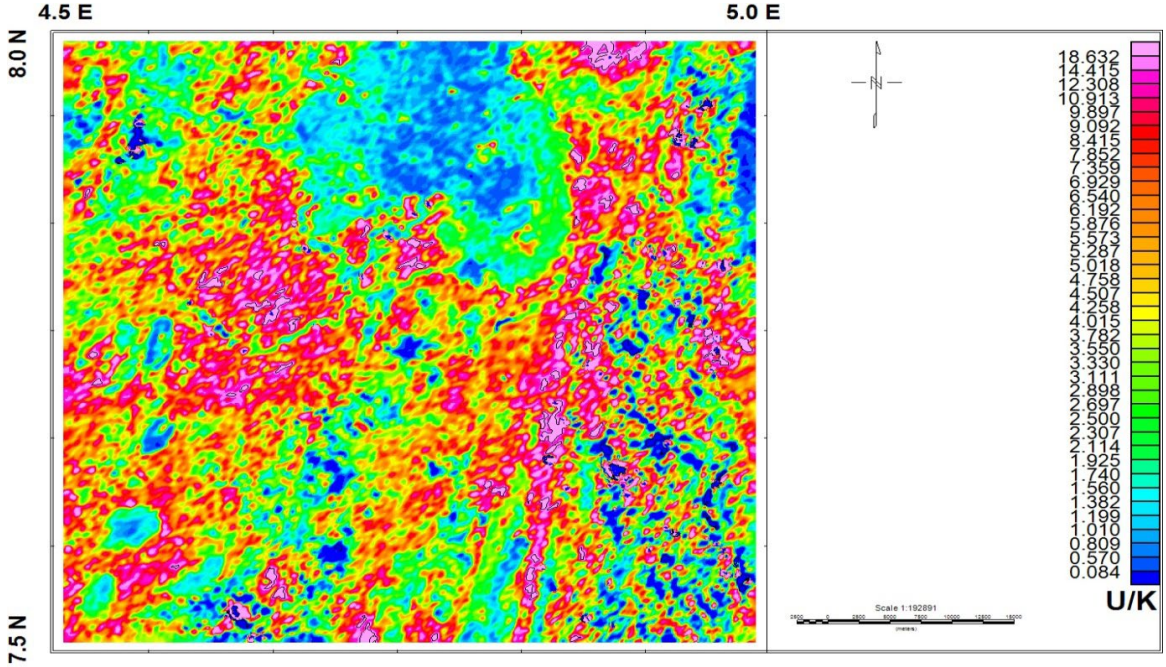

Figure 5: *Airborne radiometric ratio of uranium to potassium (U/K) anomalies of the study area.*

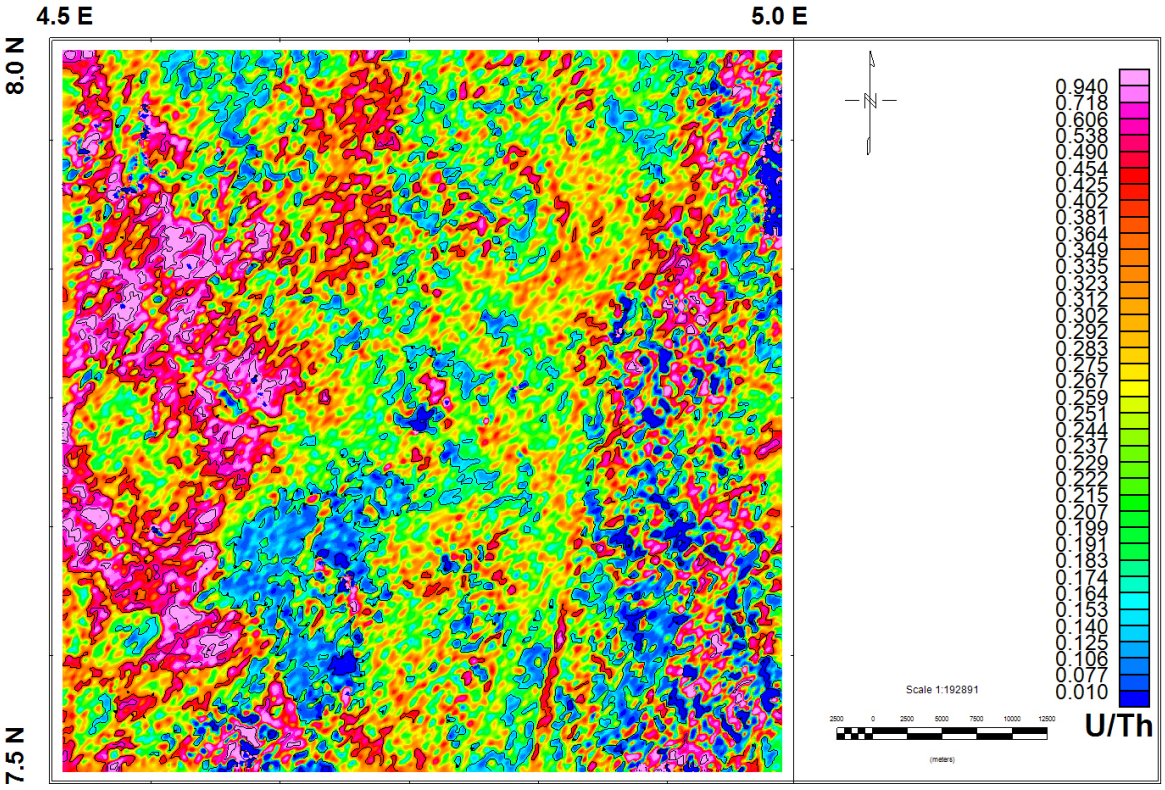

Figure 6: *Airborne radiometric ratio of uranium to thorium (U/Th) anomalies of the study area.*

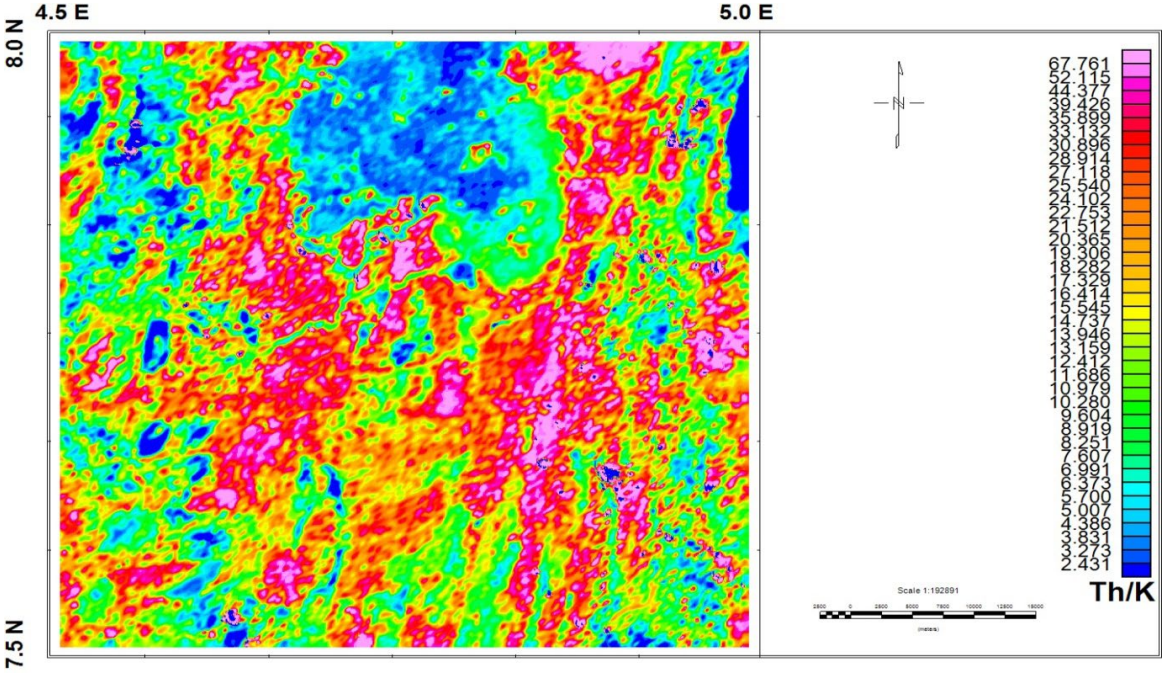

Figure 7: *Airborne radiometric ratio of thorium to potassium (Th/K) anomalies of the study area.*

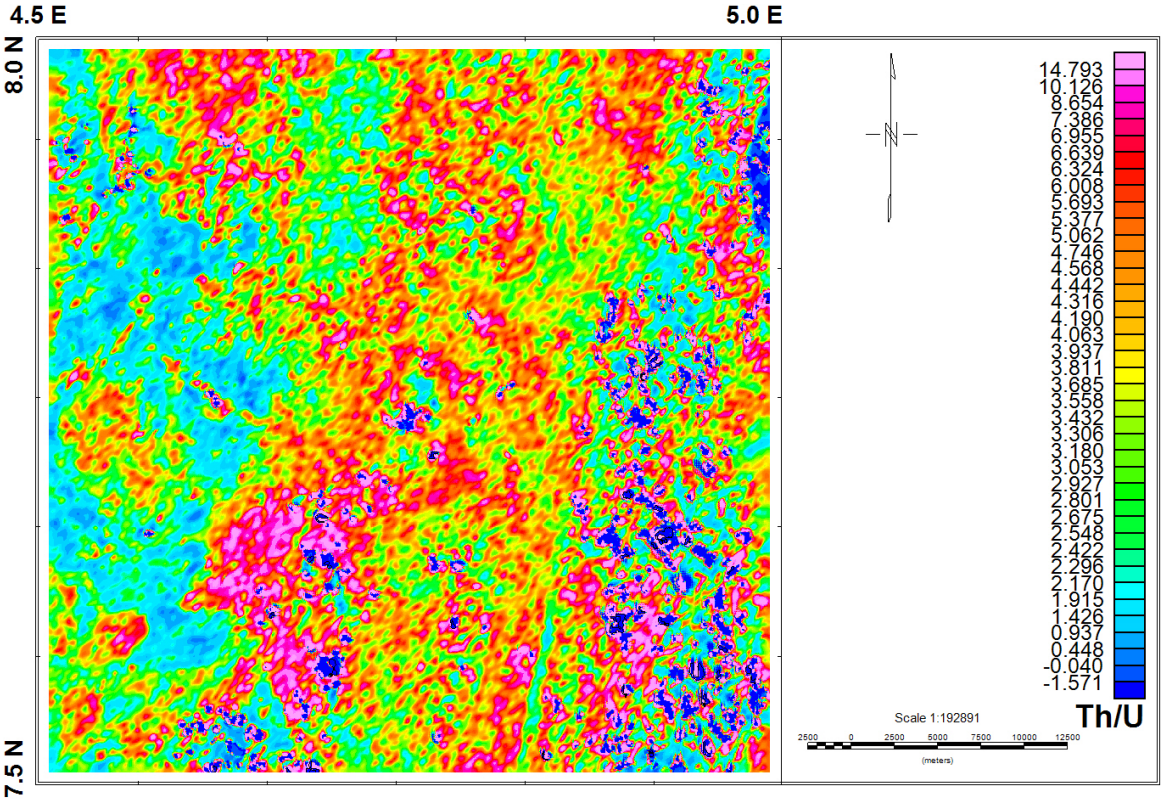

Figure 8: *Airborne radiometric ratio of thorium to uranium (Th/U) anomalies of the study area.*

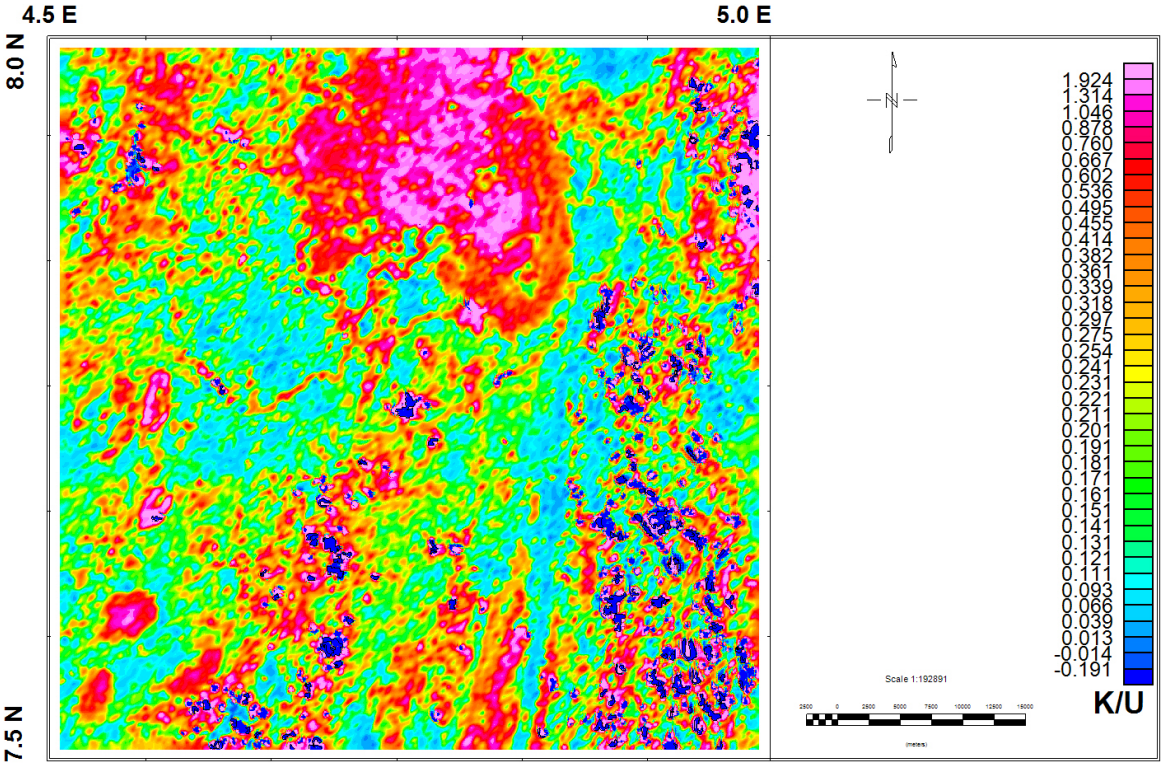

Figure 9: *Airborne radiometric ratio of potassium to uranium (K/eU) anomalies of the study area.*

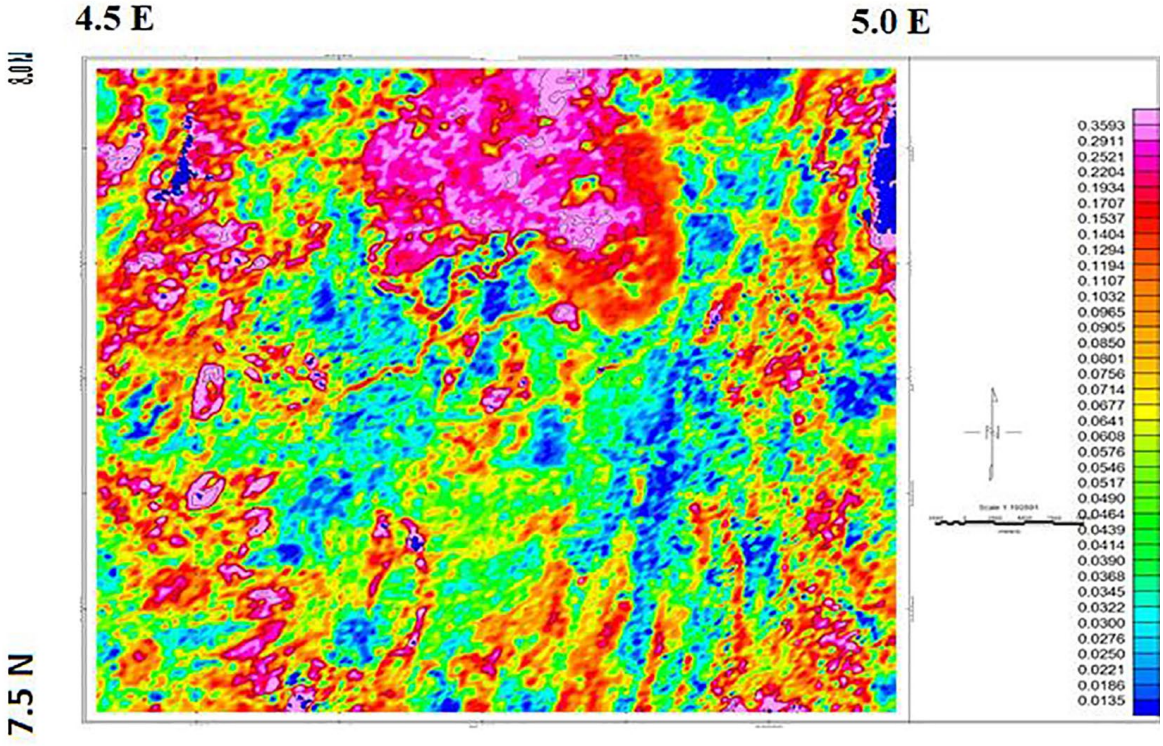

Figure 10: *Airborne radiometric ratio of potassium to thorium (K/Th) anomalies of the study area.*

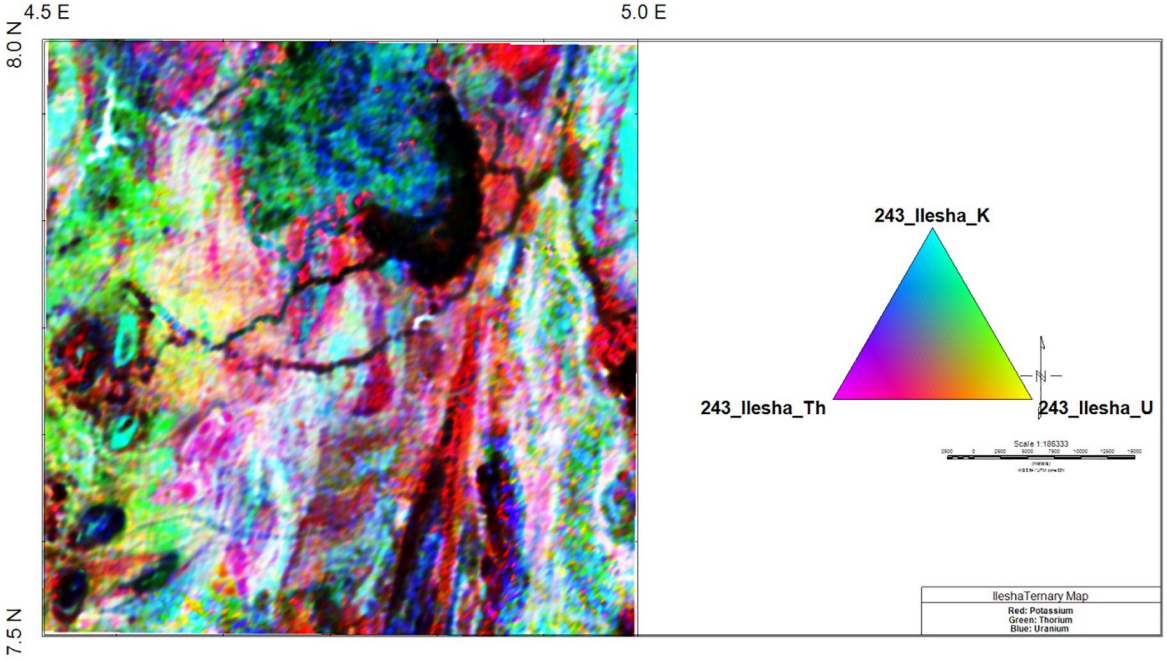

Figure 11: *Airborne radiometric of thorium (Th), uranium (U) and potassium (K) in RGB ternary image of the study area.*

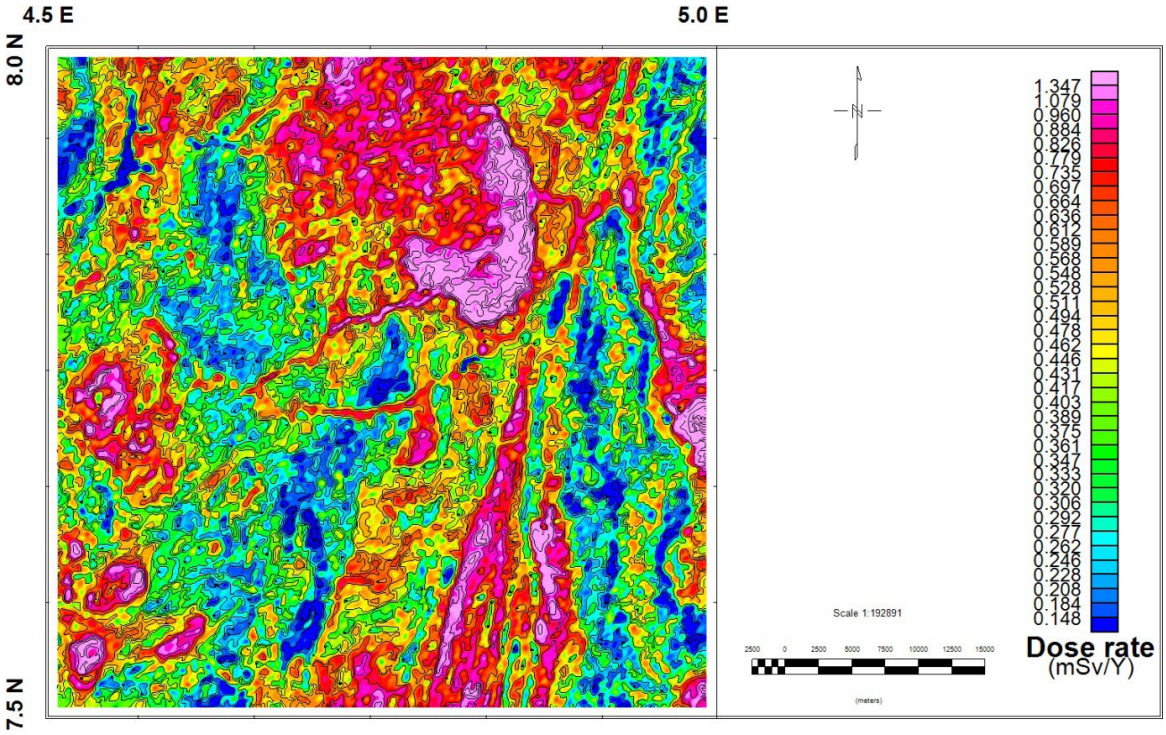

Figure 12: *Radioactivity dose rate contour map of the study area.*

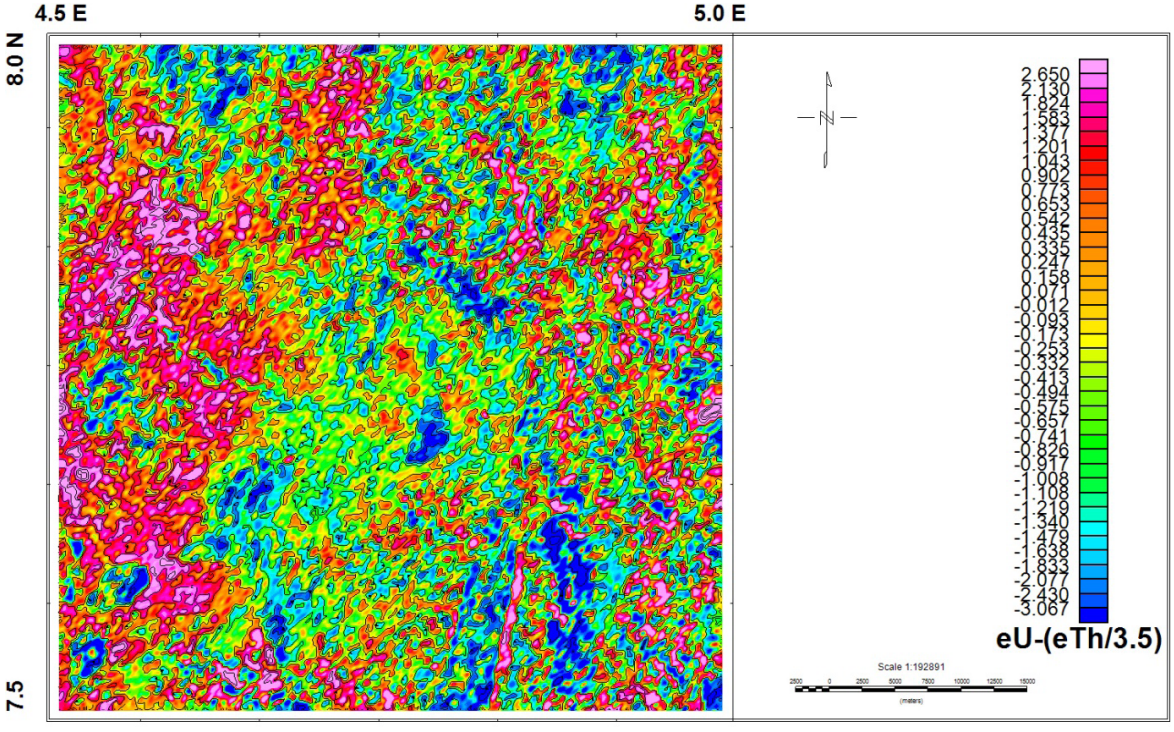

Figure 13: *Uranium migration index contour map of the study area.*

Table 1: *Summary of statistical results.*

	eTh (ppm)	eU (ppm)	K (%)	Dose rate (mSv/yr)	Composite/total counts (Ur)
Average	10.6	2.85	0.91	0.522	14.52
Minimum	0.11	0.1	0.15	0.182	2.27
Maximum	76.49	37.79	3.56	3.93	26.72
Standard deviations	6.8	1.91	0.90	0.31	8.60

be 10.60 ± 6.80, having the minimum value of 0.11 ppm and the maximum value of 76.49 ppm (Table 1); one of the stable thorium minerals was monazite, which could be assumed to be present [19].

The equivalent concentration uranium contour map

From the equivalent concentration uranium contour map in Figure 3, it can be found that there were relatively four levels of radioactivity with characteristic geological representation of undifferentiated schist amphibolite meta-volcanic with pegmatite complex and quartzite/quartz schist for levels between 0.08 and 1.35, granite gneiss/porphyritic granite for levels between 0.10 and 2.57, schist/branded gneiss for levels between 2.57 and 4.93 and lastly, branded gneiss for the level with the highest value of equivalent uranium radioactivity between 4.93 and 37.79 ppm, which was in agreement with the earlier work by [19]. There is a high difference in this last range. The average value of equivalent uranium concentrations in the study area from Table 1 is 2.85 ± 1.91, ranging from 0.10 to 37.79 ppm; it could be assumed that zircon mineral may be present in these areas since it is a stable uranium mineral.

The potassium % contour map

The plot of the distribution of potassium (%) in the study area shows that the area is enriched with potassium (%), which corresponds to porphyritic granites in the geological map of the area. Some parts such as the northwest, northeast and south are also relatively rich in it.

The levels of this radioactivity from the contour map in Figure 4 were shown to be from 0.15 to 0.30, 0.30 to 0.54, 0.54 to 1.94 and 1.94 to 3.56, which corresponded to geological representations of banded gneiss, undifferentiated schist amphibolite meta-volcanic with pegmatite complex, granite gneiss and pegmatite/quartz vein and the highest porphyritic granite formations, respectively. The average value of potassium (%) in the study area found from Table 1 is 0.91 ± 0.90%, having a minimum value of 0.15% and a maximum value of 3.56%.

The contour map of eU/K ratio

The contour map of eU/K ratio shown in Figure 5 reveals that the area has eU/K ratio >1 in almost all the study areas except at porphyritic granite areas where the values are ≤ 0.8.

The contour map of eU/eTh ratio

Looking at the contour map of eU/eTh ratio (Figure 6), it was noticed that the radioactive level of eTh was higher than that of eU, as the ratios are less than 1. eU/eTh ratio dominates the western part with characteristic geology of pegmatite/quartz vein, granite gneiss, metadiorite and some parts of schist zones and also a few places in the eastern part with characteristic feature of migmatite representations. The ratios of eU/eTh are lowest around the central parts (undifferentiated schist amphibolite meta-volcanic with pegmatite complex).

The contour map of eTh/K ratio

Figure 7 shows that there are more eTh contents than potassium contents. It can be seen that the values decrease where there are highest contents of potassium at the porphyritic granite areas, whereas the ratios are high at granite gneiss, banded gneiss, undifferentiated schist amphibolite meta-volcanic with pegmatite complex and some parts of quartzite/

quartz schist geological representations. These areas are enriched in thorium.

The contour maps of K/eU, K/eTh and eTh/eU ratios

The ratios of eTh/eU, K/eU and K/eTh are shown in Figures 8–10, respectively. In Figure 8, the theoretically expected ratio of thorium to uranium for normal continental crust is approximately 3.0, which shows that no significant fractionalisation occurs during weathering and there is no involvement in metasomatic activity of the radioelement. Figure 8 also shows that uranium leaching occurs. Potassium abundance is measured directly as gamma rays are emitted when ^{20}K decays to argon, uranium and thorium and cannot be measured directly. The granitic rocks with little soil cover could be easily identifiable with high concentrations of K and Th, whereas the same granitic bodies with thick soil cover show negative anomalies than the granitic terrain. The value of the ratios of eTh/eU, K/eU and K/eTh ranges between -1.571 and 14.793, -0.191 and 1.924 and 0.0135 and 0.3593, respectively.

The composite (total count) contour map of the radioelements (Ur)

The composite image of the radioelements combines all the three data, K (%), eU and eTh, in Figure 11; this is also the total count contour map. At the lower part of the porphyritic granite around Imesi Ile and Ilare, a high concentration of the three radioelements is shown. eU, K and eTh occur at high concentrations in fresh granite soil and in granite soil where clay layers are close to or exposed at the surface [24].

The northwestern region through southwestern parts shows more thorium, the northeastern region through the middle region shows more potassium contents and towards the extreme northwest and some parts of the south-south, uranium contents are dominated.

The average total count in the study area is 14.52 ± 8.60, with the minimum value of 2.27 and the maximum total count (Ur) of 26.76.

Equivalent dose rates of the study area

The study to determine environmental dose rates in Ilesha was carried out using Equations (1) and (2) in order to quantify the radiological relevant doses to ascertain that the environment of the study area does not pose any harm to the public. Figure 12 shows the contour map. The areas with high environmental dose rates fall within the granite gneiss, banded gneiss and some migmatite areas with some relatively high dose rate areas around the porphyritic lithological areas. The areas with low environmental doses fall within undifferentiated schist amphibolite meta-volcanic with pegmatite complex and some parts of quartzite/quartz schist areas. It has been known from studies that igneous rocks of granite compositions are really enriched in thorium and uranium contents compared to rocks of ultramafic or basaltic composition [25]. Some shales and phosphate rocks too are exceptions [26].

The range of the dose rates calculated in the study is between 0.1817 and 3.9296, having an average value of 0.5222 ± 0.3106 mSv/yr. Places like Imesi Ile, Ilare, Idi-Aba, Tonkere, Ipole, Kewo, Iree, Odo-Igba, Boluwaduro and Ikogosi are around the high dose rate areas. This could be attributed to the outcrops in the area since outcrop areas are known to have high background radiations as a result of the basement complex rock formation. These areas are still comparable with places that are known to have high background radiations such as Abeokuta and Jos in Nigeria [27,28]. The average dose rate for the study area is still below the recommended safe limit of 1 mSv/yr for natural radiation sources in the environment [26]. The areas with anomalies should be subjected to further studies using other techniques.

The contour map of uranium migration index (ppm)

The uranium migration index was calculated to study the migration of uranium into and out of the different geological regions' migration index. There was depletion of uranium along the fault line of undifferentiated schist amphibolite meta-volcanic with pegmatite complex around Dumuye village as shown in Figure 13 and also mostly around the centre of the study area with characteristic geology of quartzite/quartz schist. The areas with negative values of uranium trends from northwest to southwest within the area under consideration majorly have uranium deposition as these regions have pos-

itive values of the index. Schist, granite gneiss, branded gneiss and few parts of undifferentiated schist amphibolite meta-volcanic with pegmatite complex fall under these regions, with places such as Ora, Igbona, Idi-Aba, Tonkere, Bara, etc.

Magnetic data processing

Airborne magnetic data were subjected to magnetic automated gradient technique in order to emphasise magnetic features from sources in both shallow and deep geologic environments. The purpose of the enhancements was to transform anomalies into forms that can be directly compared with important rock mineralogical properties. This process correctly positioned anomalies over their causative sources, increased the resolution of small-scale anomalies related to near-surface magnetic sources and converted data to a model of magnetic susceptibilities for comparison with rock mineralogical properties.

Horizontal Gradient

The horizontal gradient method (HGM) is in many ways the simplest approach to estimating contact locations and depths. It requires the greatest number of assumptions about the sources but is the least susceptible to noise in the data, because it only requires calculation of the first-order horizontal derivatives of the magnetic field. If *T(x, y)* is the magnetic field, then the horizontal gradient magnitude *HG(x, y)* is given as follows:

$$HG(x,y) = \sqrt{\left(\frac{dT}{dx}\right)^2 + \left(\frac{dT}{dy}\right)^2 + \left(\frac{dT}{dz}\right)} \qquad (4)$$

This function peaks over magnetic contacts under the following assumptions: (1) the regional magnetic field is vertical, (2) the source magnetisations are vertical, (3) the contacts are vertical, (4) the contacts are isolated and (5) the sources are thick. Violations of the first four assumptions can lead to shifts in the peaks away from the contacts. Violations of the fifth assumption can lead to secondary peaks parallel to the contacts. In order to partially satisfy the first two assumptions, it is usually necessary to perform transformation known as pseudo-gravity on the observed magnetic field. Crests in the horizontal gradient magnitude can be located by passing a small 3 × 3 window over the HGM grid and searching for maxima [29]. The 1997 programme HDEP [30] used a similar approach within a 5 × 5 window to both locate the crests and determine their strike direction. Once a crest is located and the strike direction is known, data within the window and within a belt perpendicular to the strike can be used to determine the depth of the contact by performing the least-squares fit method to the theoretical shape of the HGM over a contact. If h is the horizontal distance to the contact, d is the depth to the top of the contact and k is a constant, then the theoretical curve is given by the following equation [31]:

$$HG(h) = \frac{k}{h^2 + d^2} \qquad (5)$$

The least-squares fit method gives an estimate of both the depth and its standard error, which can be expressed as a percentage of the depth. Typically, only depth estimates with standard errors of 15% or better are retained in the final interpretation. The HGM is relatively insensitive to noise in the data and interference effects between nearby sources.

Analytic signal amplitude (ASA)

Analytic signal (AS) is a transform formed through the combination of horizontal and vertical gradients of a magnetic anomaly. In 1972 and 1974, Nabighian [32,33] involved the concept of the AS for magnetic interpretation and showed that its amplitude yields a bell-shaped function over each corner of a 2D body with polygonal cross-section.

AS is defined as

$$A(x,y) = \frac{dT}{dx}i + \frac{dT}{dy}j + \frac{dT}{dz}k \qquad (6)$$

where i, j and k are unit vectors in x, y and z directions, respectively. The real and imaginary parts of its Fourier transform are horizontal and vertical derivatives of T.

In the frequency domain, the amplitude of the AS of the total magnetic field T is calculated from the three orthogonal derivatives of the field [34]. The absolute value or amplitude A

of the simple AS is given by the following equation:

$$|A(x,y)| = \left[\left(\frac{dT}{dx}\right)^2 + \left(\frac{dT}{dy}\right)^2 + \left(\frac{dT}{dz}\right)^2\right]^{1/2} \quad (7)$$

Equation 7 shows that the location of the source in the horizontal plane can be deduced from the peak position of the amplitude of the AS and the source depth can be estimated as the half width of the half maximum of the amplitude of the AS. This function acts as envelope of all possible phase shifts of an observed anomaly and peaks over magnetic contacts, regardless of the regional magnetic field direction, the source magnetisation and the dip of the contact. It was pointed out by Roest et al. [35] that depth can be estimated from the shape of the AS based on non-linear curve fitting; solving the non-linear problem is always difficult. The contact depth model can therefore be calculated from the AS using the 2D expression of the AS magnitude for a model given by the following equation [36]:

$$AS(x) = \frac{k}{(x^2 + z^2)^{\frac{1}{2}}} \quad (8)$$

where k is the magnetisation constant and z the depth to the top of contact.

Local wavenumber (LWN) method

The phase angle is defined as the angle between the vertical derivative and the absolute value of the total horizontal derivative of the potential field data, which in edge detection context is termed as tilt angle [37]. In this study, we analysed depth estimates derived using the LWN. The determination of the local phase (LP) and LWN for grid-based data have been made easier using the methods reported by Fairhead et al. [38] and Verduzco et al. [39]. In 1965, Bracewell [40] defined f (the local frequency) as the rate of change of LP with respect to x. Thus, f can be expressed mathematically as given in the following equation:

$$f = \frac{1}{2\pi}\frac{\partial}{\partial x}\tan^{-1}\left[\frac{\frac{\partial T}{\partial z}}{\frac{\partial T}{\partial x}}\right] \quad (9)$$

Defining the LWN in terms of frequency,

$$k = 2\pi f \quad (9)$$

Substituting Equation (9) into Equation (10) leads to the following equation:

$$k = \frac{1}{|A|^2}\left(\frac{\partial^2 T}{\partial x \partial z}\frac{\partial T}{\partial x} - \frac{\partial T}{\partial x^2}\frac{\partial T}{dz}\right) \quad (10)$$

For gridded data, it has been shown by Huang and Versnel [41] that the wavenumber is given by

$$k = \frac{1}{T_x^2 + T_y^2 + T_z^2}$$

$$\times \left\{T_x\left[T_{xx} - \frac{T_z}{T_x^2 + T_y^2}\left(T_x . T_{xx} + T_y . T_{xy}\right)\right]\right. \quad (11)$$

$$\left. + T_y\left[T_{xy} - \frac{T_z}{T_x^2 + T_y^2}\left(T_x .* T_{xy} + T_y\ *. T_{yy}\right)\right]\right\}$$

By considering a sloping contact, the expressions for the vertical and horizontal gradients as defined by Nabighian [32] are given by

$$\frac{\partial T}{\partial z} = 2sFc\sin d$$

$$\frac{x\cos(2I - d - 90) - h\sin(2I - d - 90)}{h^2 + x^2} \quad (12)$$

$$\frac{\partial T}{\partial x} = 2sFc\sin d$$

$$\frac{h\cos(2I - d - 90) - x\sin(2I - d - 90)}{h^2 + x^2} \quad (13)$$

where s is the susceptibility contrast, F the magnitude of the ambient field, , a the ambient field declination, I the inclination of the ambient field, d the angle of dip of the body and h the depth to the top of the contact.

Substituting Equations (12) and (13) into Equation (10), we have Equations (14), (15) and (16), which are the required source parameters, namely, magnetic contact depth, local dip and local susceptibility, respectively.

$$k = \frac{h}{h^2 + x^2} \quad (14)$$

Let $x = 0$ and the peaks coincide with the edges of the bodies, then local depth can be written as

$$h = \frac{1}{k} \quad [8] \ (15)$$

and

$$K = \frac{|A|}{k2kcSind} \quad (16)$$

Magnetic data interpretation

According to Poirier [42], the main use of high-resolution airborne magnetic maps and their derivatives in mineral prospecting is to make geological deduction from them. The total magnetic intensity grid was created using a minimum curvature gridding algorithm with a grid cell size of 50 m. The grid values fit the profile data to within 1 nT for 99.98% of the profile data points. The average gridding error is well below 0.1 nT. The total magnetic intensity map of the gridding of sheet number 243 is shown in Figure 12.

From the range of magnetic intensity values of these data, information on subsurface lithology, trend and geological structures can be obtained. Quantitative interpretation approach was adopted for the mapping of basement topography around Ilesha, southwestern Nigeria, with the aim of establishing depth to basement in the basement complex. The total magnetic field intensity map of Ilesha and its environs is presented in Figure 14. The total magnetic field intensity map indicates high magnetic intensity values in the north, west, northwestern, southeastern and the central part of the area under consideration (Imesi Ile, Ilare, Idi-Aba, Tonkere, Ipole, Odo, Odo Ibga and Ikogosi). The total magnetic intensity value of the field ranged from –79.41 to 140.93 nT with a range of 220.34 nT between the lowest and highest intensity points, suggesting contrasting rock type in the study area. Regions of magnetic lows (low-amplitude magnetic anomaly) and highs (high-amplitude magnetic anomaly) are apparently revealed on the magnetic map (Figure 15). The northern and western regions of this map are characterised by relatively high-amplitude magnetic intensity values (16.93–140.93 nT) with intrusion of low magnetic intensity signature that coincides with ferruginous quartzite and the Precambrian crystalline basement rocks of southwestern Nigeria on the surface geological map (Figure 1), whereas the southeastern area with relatively low-amplitude magnetic intensity values (–79.41–2.58 nT) coincides with relatively thick sedimentary cover, where the effect of the thick weakly susceptible materials masks the high magnetic susceptibility from relatively deep basement rocks.

Figure 15 shows the effect of the application of reduction to the magnetic equator filter operation, the filtering attempts to centre some of the wrongly horizontally elongated anomalies due to low latitude effects. The reduction to equator (RTE) map shows that the correction in the asymmetries of the observed anomalies had been minimised, and it centres the anomalies directly over the causative elongated bodies. The reduction in magnetic intensity values of the equator map ranged from –64.62 to 133.09 nT. The reduction to the equator map is characterised by high frequency, short wavelength, small size, weak intensity, sharp low amplitude and nearly irregular-shaped anomalies, which may be due to near-surface sources, such as shallow geologic units and cultural features.

The second vertical derivative filter was applied to the airborne magnetic data of the study area to improve local anomalies obscured by broader regional trends. It accentuates short-wavelength components of the anomaly field, while de-emphasising long-wavelength components. The output of its application in the study area is shown in Figure 16.

AS map of Ilesa (Figure 17) was derived from AS grid computed from 1st-order vertical derivative values of two horizontal gradients and one vertical gradient of the magnetic intensity of the sheet number 243. AS map of the study area (sheet number 243) shows the amplitudes of the magnetic signature. Prominent high-amplitude AS anomalies are apparent on the AS map. The analytic function acts as the envelope of possible phase shift of the observed anomaly

and peaks over magnetic contacts. The AS map also shows the attenuation of shallow sources. Some regions in the map are characterised by very high amplitude, which reflects lithological variation in magnetic basement, while some parts of the study area is dominated by low amplitude and indicates presence of thick sediment covering the weathered basement. The magnitude of amplitude of magnetic gradient intensity ranges from 0 to 2.8 nT/km.

The sources' location and magnetic contact depth solutions were computed by HGM of RTE grid, ASA of total magnetic intensity grid, and local wavenumber (LWN) of total magnetic intensity grid using a maximum standard error of 15%. Depths on sheet number 243 (Ilesha) are shown in Figures 18–20, respectively, for HGM of RTE grid, ASA, and LWN.

The HGM assumes that the sources are isolated vertical contacts separating thick geologic units and that the magnetisation vectors are collinear with the geomagnetic field vector. Peaks in the horizontal gradient magnitude of the RTE magnetic field indicate the location of the contacts and estimate their strike directions in the depth map as shown in Figures 18–20. In addition, peaks in the ASA and LWN, which is derived from the first horizontal and vertical derivatives of the observed magnetic field, indicate the location of the contacts and estimate their strike directions.

The results obtained indicate that HGM records the highest number of contacts with 113 solutions at comparatively deeper depths than other methods. The results obtained from the HGM revealed depth range limit of 0.478–4.112 km, while the AS gave an estimated depth to the magnetic sources ranging from 0.348 to 2.551 km. The LWN method revealed an estimated depth ranging from 0.478 to 5.48 km. The solutions from HGM and analytical ASA functions are comparable and better than the solutions from the LWN. In each diagram (Figures 18–20), the centre of each circle coincides with the location of maximum for that function and the diameter of the circle is proportional to the depth estimate for the source point of the anomalies. The direction of the diameter indicates the strike direction of the lineament. LWN overestimates the source depths relative to other methods; otherwise, the three results contain similar features, which is in agreement with earlier works by [43] and [44].

Table 2: *Magnetic susceptibility values of minerals [46].*

Minerals	Magnetic susceptibility (10^{-6}) SI
Andradite	2,280–4,320
Staurolite	790–1,590
Cordierite	200–1,100
Tourmaline	39–1,520
Beryl	23
Epidote	1,010
Orthite	970–960
Zircon	–15–386
Opal	–12.9
Orthoclase	–13.7
Halite	–10.3
Calcite	–10–100
Quartzite schist	140–220
Pegmatite	90–370
Muscovite tourmaline	10–120
Gneiss	164–260
Limestone	4–20
Sandstone	0.2–5
Gabbro	200–420
Augite	17–100
Haematite	2,150–5,100
Schist	213–469
Tourmaline	20–79
Sphene	264
Actinolite	100–990
Hornblende	764–1368
Pyrite	-6.3–63
Galena	-33–9.3
Dolomite	14–23
Garnet	10–56
Quartz	-6.3
Graphite	-4–76
Biotite	100–307

A close examination of the maps of HGM, ASA and LWN in Figures 18, 19 and 20, respectively, reveals the differences in the diagnostic attributes of these functions. The resolution of HGM and ASA is comparable, while that of the LWN map is least. The apparent magnetic susceptibility values were estimated using the filter operator in Oasis montaj™ [45], a software package for potential data processing. The apparent susceptibility values of the study area (sheet number 243) ranged from -0.00325 to 0.00323

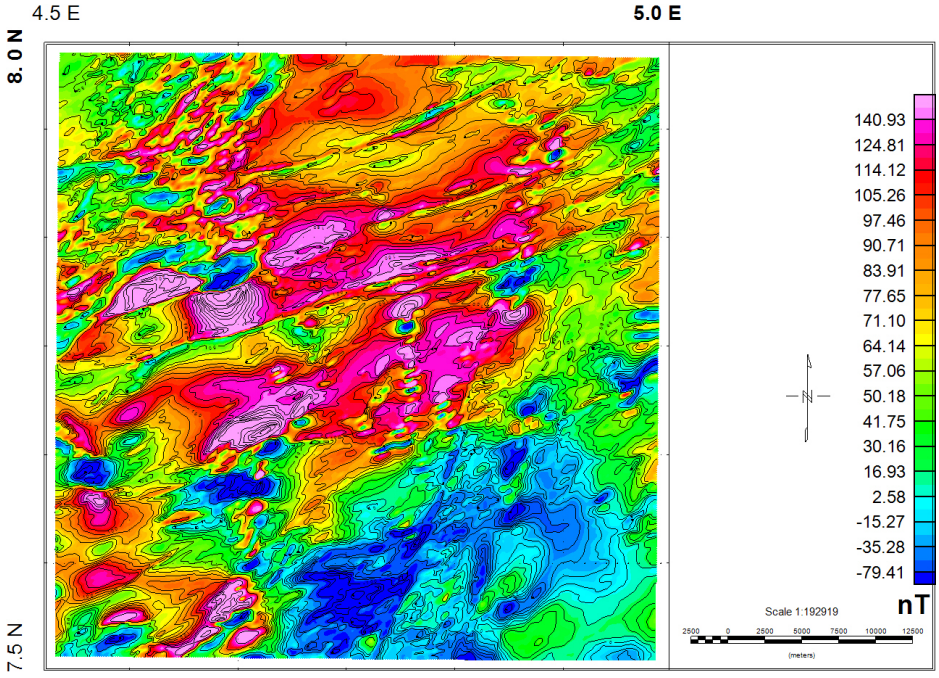

Figure 14: *Total magnetic intensity map of Ilesha and its environs.*

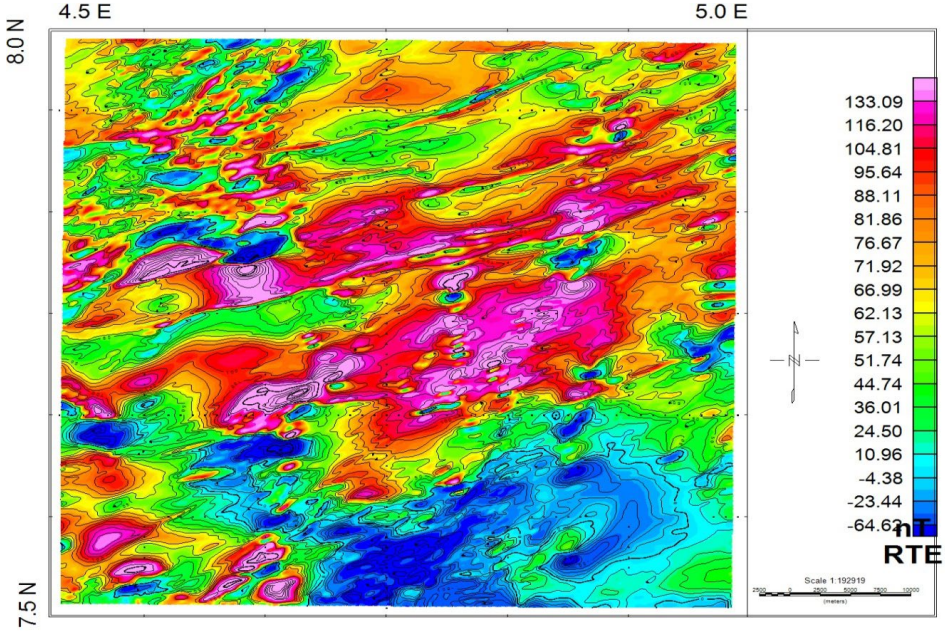

Figure 15: *Total magnetic intensity map of study area after reduction to equator.*

as shown in Figure 21 suggesting contrasting rock types. The northern, southern, southeastern and northwestern regions of this map are characterised by relatively high susceptibility values ranging from 0.00061 to 0.00323, which could be inferred as areas where the fibre-grained quartzite schist, muscovite, tourmaline gneiss and pegmatite are concentrated in the deposit, whereas the southwestern region is characterised by relatively low apparent susceptibility values ranging from -0.0004 to 0.00058, which could be inferred as a weathered and fresh basement area.

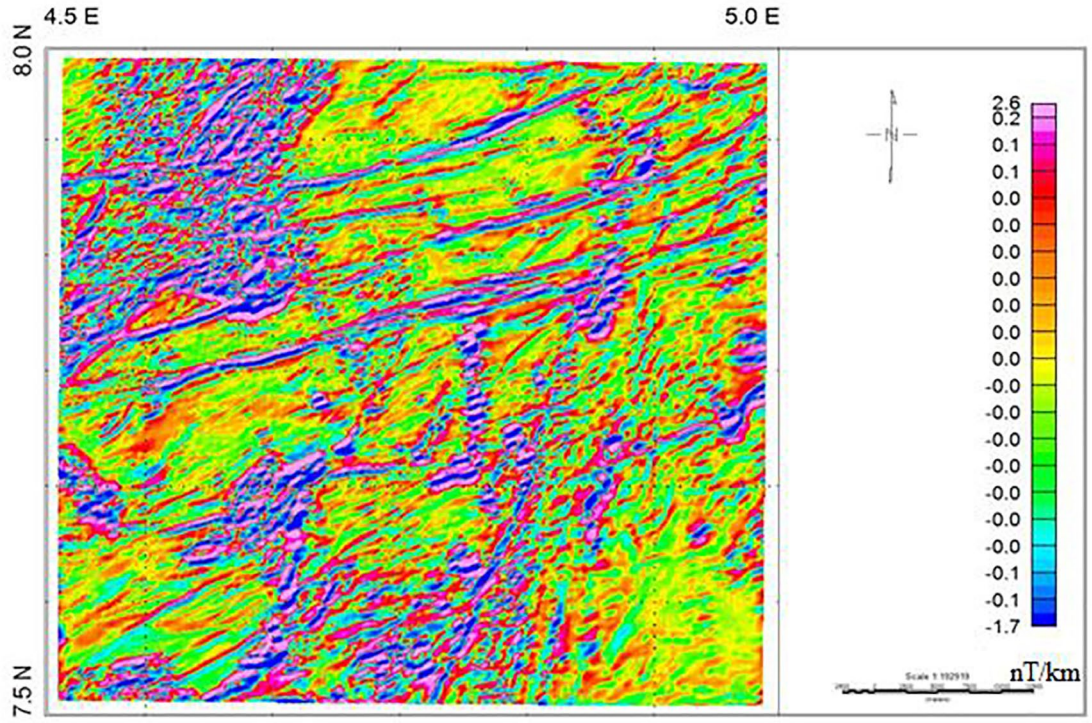

Figure 16: *Vertical gradient map of the study area.*

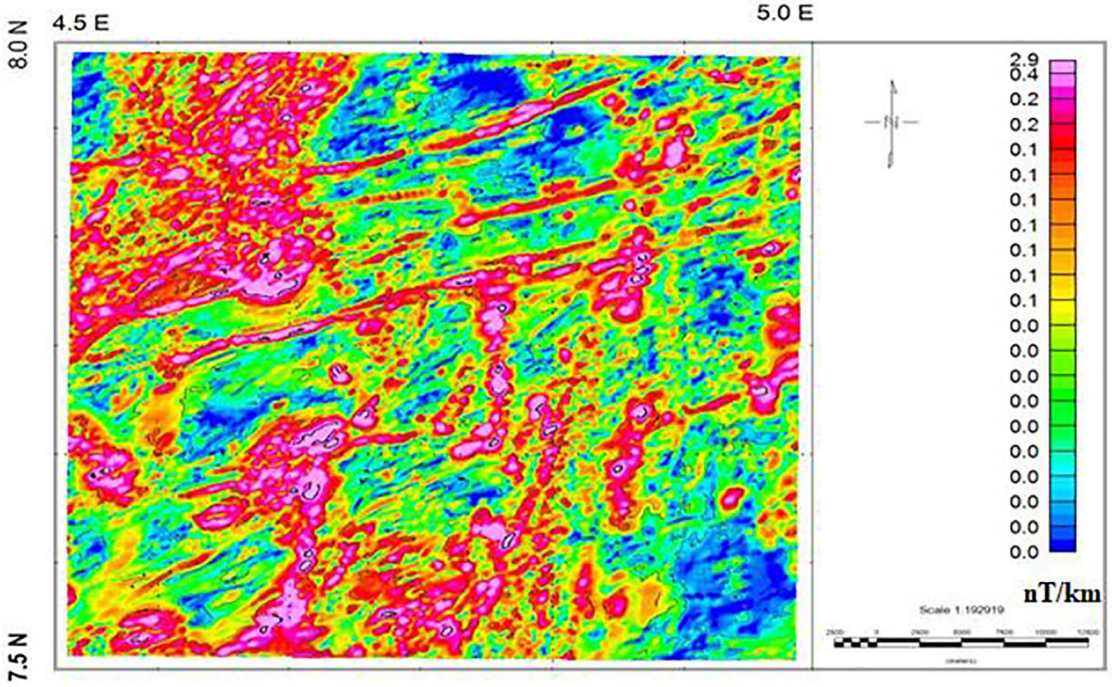

Figure 17: *Analytical map of the study area.*

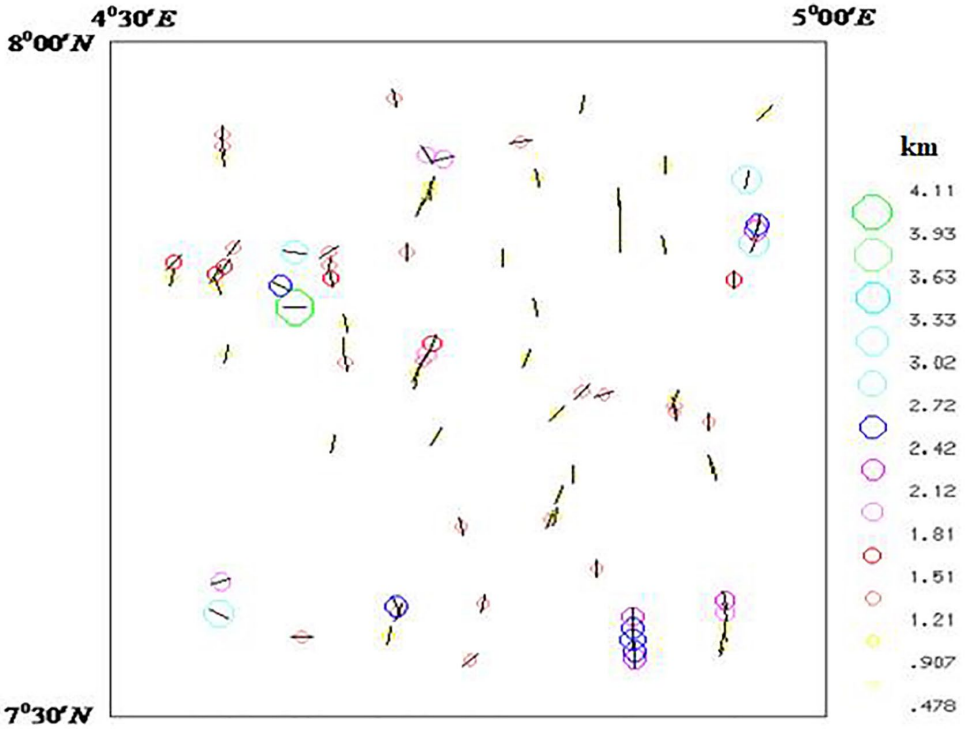

Figure 18: *Horizontal gradient depth map of Ilesha and its environs.*

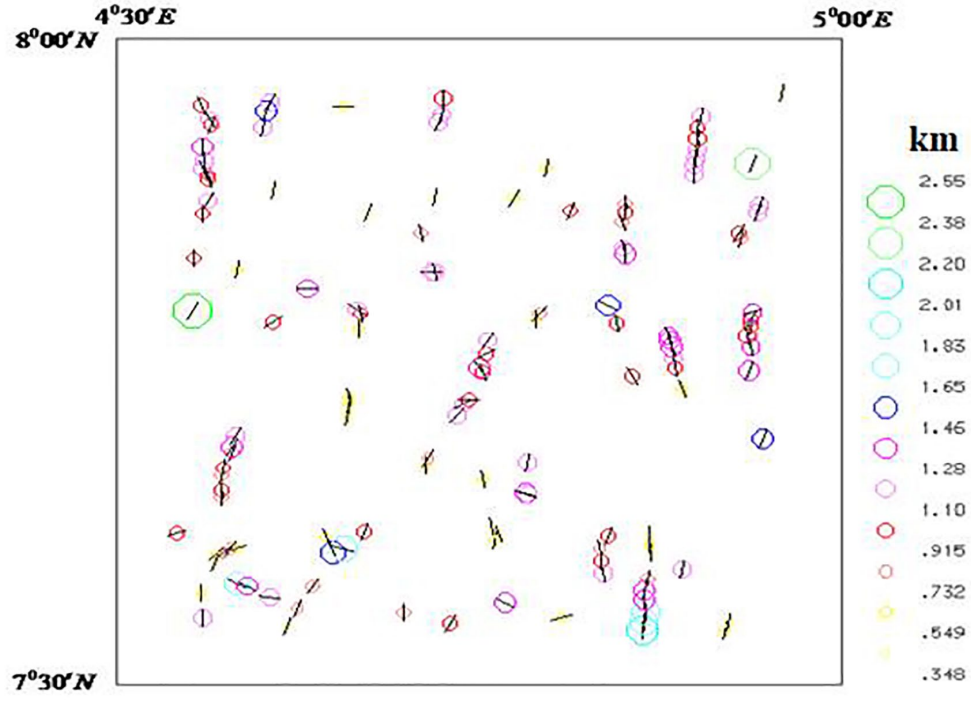

Figure 19: *AS magnitude depth map of the study area.*

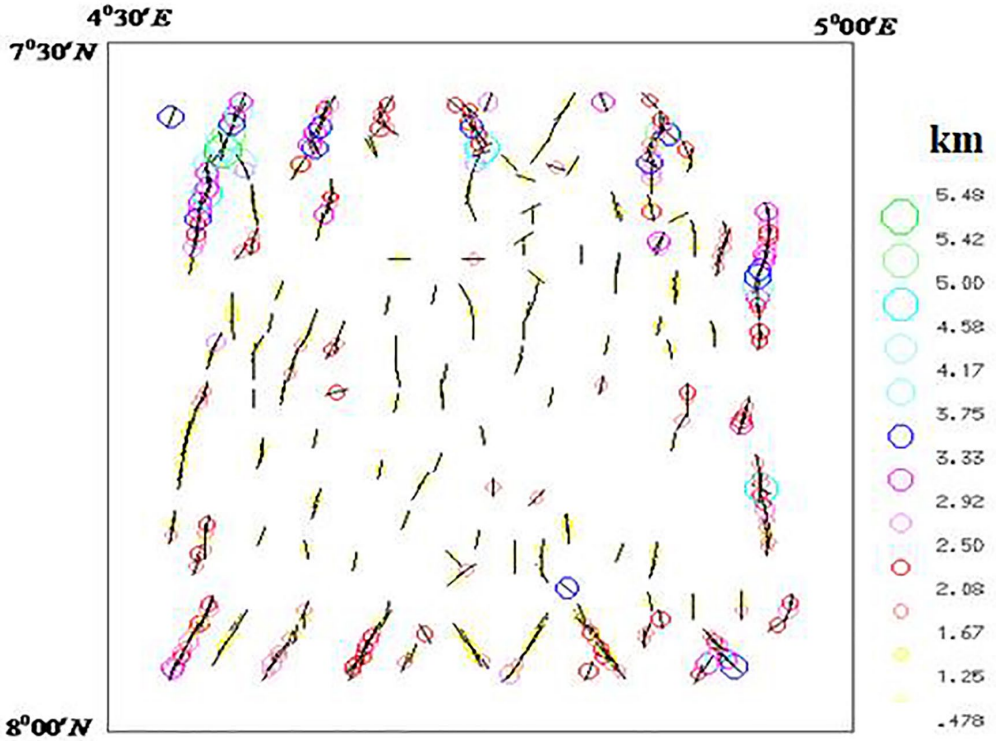

Figure 20: *LWN depth map of Ilesha and its environs.*

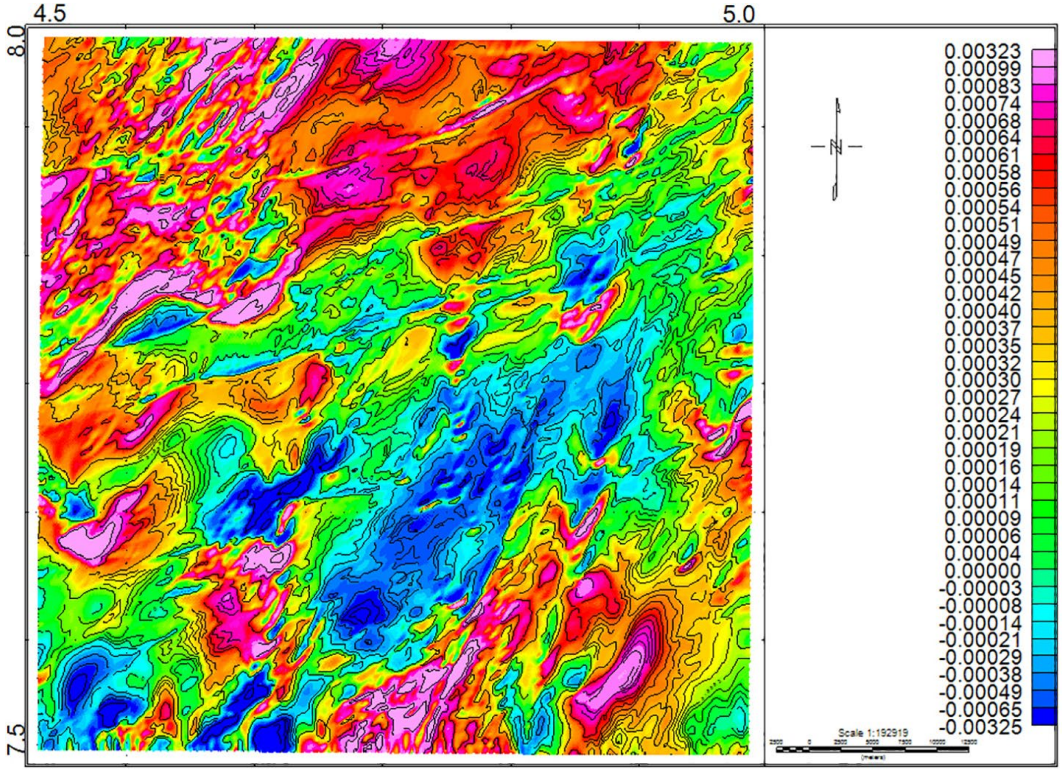

Figure 21: *Apparent susceptibility map of Ilesha and its environs.*

Conclusion

The study of the nature of the distribution of the three radioelements has been carried out using radiometric data. The distribution of the three radioelements with the geological structures of the area has been studied, and it was noted that the maximum values of eU and eTh (ppm) fall within the branded gneiss regions, while the maximum values of K (%) fall within the porphyritic granite region. Equivalent thorium has the highest radioactive content. The mean environmental radioactivity dose rates of the study area were found to fall within the acceptable safe limit of 1.0 mSv/yr, although there are places with high values. Ratios of the radioelements (eU/K, eU/eTh and eTh/K) have been analysed to check whether there was an enrichment or depletion of radioisotopes [25] in the area, and it was found that eU/eTh is less than 1 since eTh is higher than eU, indicating depletion in uranium, whereas eTh/K is greater than 2, indicating equivalent thorium enrichment.

The airborne magnetic data have been analysed using three automated gradient techniques, namely, HGM, ASA and LWN. In addition, the apparent susceptibility filtering technique was used to estimate apparent magnetic susceptibility of the anomaly within the area under consideration. These techniques have been adopted to delineate Ilesha area in order to gain understanding and interpretations. The value of magnetic intensity distribution in the field ranged from -79.41 to 140.93 nT, and it was found to depend on the size, depth of burial and the thickness of the low susceptibility superficial material overlying the magnetite crystalline rocks within the study area. High magnetic intensity values characterised the basement rocks, whereas lower magnetic intensity values distinguished metasedimentary rocks and fresh basement. The results revealed that a basement rock occurs in all parts of the study area. The location and depth to magnetic contacts have been estimated from the peak of the HGM, LWN and ASA functions of the total intensity magnetic data. The results of this study have shown that the estimates of depth limit to shallow magnetic contact by HGM and ASA methods are relatively close and comparable.

The LWN method overestimated the depth to the shallow sources and revealed a smaller depth for the shallow sources. The shallower depth, ranging from 0.382 to 0.478 km, may refer to some major magnetic units, uplifted basement surface and some local magnetic features. These results therefore demonstrate the applicability of the three gradient techniques of magnetic interpretation in estimating depths to the surface of magnetic basement in a basement complex. The obtained apparent susceptibility of the entire Ilesha and its environs ranged from -0.00325 to 0.00323 SI. This study has shown that the apparent susceptibility within the study area is controlled mainly by ferromagnetic and diamagnetic minerals. The integration of airborne radiometric and magnetic results shows that the northwestern, southeastern and central parts of the study area are dominated by high dose rates and high magnetic intensity values. These high values were observed directly in radiometric and magnetic patterns.

Acknowledgement:

The authors acknowledge Nigeria Geological Survey Agency of Nigeria for releasing airborne magnetic and spectrometric data.

References

[1] El-Sadek, M.A., Ammar, A.A., Sabry, A.R. (2002): Aeroradiospectrometry in the Lithological Mapping and Environmental Monitoring of Wadi Araba Area. *The Arabian Journal for Science and Engineering*, 27(2A), pp. 131–148.

[2] Grasty, R.L., Carson, J.M., Charbonneau, B.W., Holman, P.B (1984): Natural Background Radiation in Canada. *Geological Survey of Canada Bulletin*, 360, pp. 39–60.

[3] Linden, A., Melander, A. (1986): Airborne Measurement in Sweden of the Radioactive Fallout After the Nuclear Reactor Accident in Chernobyl, USSR, Preliminary Report SGAB TFRAP 8606, 1986.

[4] Akerblom, G. (1987): Investigation and Mapping of Radon Risk Areas. In: Proceedings of the International Symposium, Geological Mapping in Service of Environmental Planning, 6–9 August 1986, F.C. Wolff (ed.), 1987.

[5] Wilford, J., Minty, B. (2006): The use of Airborne Gamma Ray Imagery for Mapping Soils and Understanding Landscape Processes. *Developments in Soil Science*, 31, pp. 207–218.

[6] Gun, P.J. (1975): Linear transformation of gravity and magnetic fields. *Geophysical Prospecting*, 23(2), pp. 300–312.

[7] Dobrin, M.B. (1976): *Introduction to geophysical prospecting*. New York: McGraw-Hill Book Company, 630 p.

[8] Thurston, J.B., Smith, R.S. (1997): Automatic conversion of magnetic data to depth, dip, and susceptibility contrast using the SPI™ method. *Geophysics*, 62(3), pp. 807–813.

[9] Coetzee, H., Larkin, K. (2011): Airborne Radiometric Surveying for the Management of Health, Safety and the Environment in the Uranium Mining Industry: Potential Applications and Limitations. B. Merkel, M. Schipek, The New Uranium Mining Boom, 483–492.

[10] De Swardt, A.J. (1953): The geology of the country around Ilesa. *Geological Survey of Nigeria Bulletin*, 23, 55 p.

[11] Rahaman, M.A. (1976): *Review of the basement geology of south western Nigeria*. In: Geology of Nigeria, Kogbe, C.A (ed.). Elizabethan: Publishing Lagos.

[12] DeSwardt, A.M.J. (1947): The Ife-Ilesa goldfield (Interim report number 2). Geology of Survey of Nigeria annual report, pp. 14–19.

[13] Russ, P. (1957): Airborne electromagnetics in review. *Geophysics*, 22, pp. 691–713.

[14] Hurley, S. (1970): Radar propagation in rock salt. *Geophysical Prospecting*, 18(2), pp. 312–328.

[15] Ajayi, T.R. (1981). On the geochemistry and origin of the amphibolites of Ife Ilesha area south west Nigeria. *Journal of Mining and Geolology*, 17, pp. 176–179.

[16] Folami, S.L. (1992): Interpretation of aeromagnetic anomalies in Iwaraja area, south western Nigeria. *Journal of Mining and Geology*, 28(2), pp. 391–396.

[17] Elueze, A.A. (1986): *Geology of the Precambranian Nigeria*. Geological Survey of Nigeria, pp. 77–82.

[18] Kayode, J.S. (2009): Vertical component of the ground magnetic study of Ijebu-Ijesa, southwestern Nigeria. A paper presented at the International Association of Seismologist and Physics of the Earth Interior (IASPEI), conference at Cape Town, South Africa; Jan 10th-16th 2009.

[19] Helmy, S.O.A., Monsour, A. Al Garni (2015): Airborne Gamma-ray Spectrometric and Magnetic Studies of Wadi Um Gehig- Wadi Abu Eligam area, Central Eastern Desert, Egypt. *Arabian Journal of Geoscience*, 8(10), pp. 8811–8833.

[20] Wilford, J.R., Bierwirth, P.N., Craig, M.A. (1997): Application of airborne gamma-ray spectrometry. *AGSO Journal Australian Geology and Geophysics*, 17(2), pp. 201–206.

[21] International Atomic Energy Agency (2003): Guidelines for radioelement mapping using gamma ray spectrometry. Vienna: International Atomic Energy Agency, 173 p.

[22] Grasty, R.L., Holman, P.B., Blanchard, Y.B. (1991): Transportable calibration pads for ground and airborne gamma –rays spectrometers. *Geology Survey of Canada*, 90, pp. 23–24.

[23] Clarke, S.P., Peterman, Z.E., Heier, K.S. (1966): Abundances in Uranium, Thorium and Potassium. In: Handbook of Physical Constants. Geological Society of America, 97: 521–541.

[24] Ramadass, G., Subbash Babu, A., Udaya Laxmi, A. (2015): Structural Analysis of Airborne Radiometric. Data for Identification of Kimberlites in Parts of Eastern Dharwar Craton. *International Journal of Science and Research*, 4(4), pp. 2375–2380.

[25] Tzortzis, M., Tsertos, H. (2004): Determination of thorium, uranium and potassium elemental concentrations in surface soils in Cyprus. *Journal of Environmental Radioactivity*, 77(3), pp. 325–328.

[26] UNSCEAR, (2000): Sources and Effects of ionizing radiation. Report to General Assembly, With Scientific Annexes, New York: United Nations.

[27] Farai, I.P., Jibiri, N.N. (2000): Baseline studies of terrestrial outdoor Gamma Dose Rate level in Nigeria. *Radiation Protection Dosimetry*, 88, pp. 247–254.

[28] Okeyode, I.C., Rabiu, J.A., Alatise, O.O., Makinde, V., Akinboro, F.G., Alhazim, D., Mustapha, A.O. (2016): Area monitoring ambient dose rate in part of southwestern Nigeria using GPS-Integrated radiation survey meter. *Radiation Protection Dosimetery*, 173(1), pp. 263–267.

[29] Blakely, R.J., Simpson, R.W. (1986): Approximating edges of source bodies from magnetic or gravity anomalies. *Geophysics*, 51(7), pp. 1494–1498.

[30] Phillips, J.D. (1997): Potential field geophysical software for P.C version 2.2. Open file report 97–725.

[31] Roest, W.R., Pilkington, M. (1993): Identifying remanent magnetization effects in magnetic data. *Geophysics*, 58 (5), pp. 653–659.

[32] Nabighian, M.N. (1972): The Analytic signal of two dimensional bodies with polygonal cross section-its properties and use for automated anomaly interpretation. *Geophysics*, 37, pp. 507–517.

[33] Nabighian, M.N. (1974): Addition comment on the analytic signal of two dimensional bodies with polyg-

onal cross section-its properties and use for automated anomaly interpretation. *Geophysics*, 39, pp. 85–92.

[34] Purucker, M. (2006): Crustal Magnetism: Geophysics, 5, Version 2.5

[35] Roest, W.R., Verhoef, J., Pilkington, M. (1992): Magnetic interpretation using the 3-D analytic signal. *Geophysics,* 57(1), pp. 116–125.

[36] MacLeod, I.N., Jones, K., Dai, T.F. (1993): Analytic signal in the interpretation of total magnetic field data at low magnetic latitudes. *Exploration Geophysics*, 24, pp. 679–688.

[37] Miller, H.G., Singh, V. (1994): Potential field tilt- A new concept for location of potential field sources. *Journal of Applied Geophysics*, 32, pp. 213–217.

[38] Fairhead, J.D., Green, C.M., Verduzco, B., MacKenzie, C. (2004): A new set of magnetic field derivatives for mapping minerals prospects. SEG 17th Geophysics (2004).

[39] Verduzco, B., Fairhead, J.D. Green, C.M., MacKenzie, C. (2004): New insights into magnetic derivatives for structural mapping: *The Leading Edge*, 23, pp. 116–119.

[40] Bracewell, R. (1965): *The Fourier transform and its applications*. New York: McGraw – Hill Book Co., 474 p.

[41] Huang, D., Versnel, P.A. (2000). Depth estimation algorithm applied to FTG data. Society of Exploration Geophysics. Expanded Abstract, pp. 394–397.

[42] Poirier, J.P. (2000): *Introduction to Physics of the earth interior*. Cambridge: Cambridge University press, 312 p.

[43] Phillips, J.D. (2010): Locating magnetic contacts; A comparison of the horizontal gradient, analytic signal, and local wavenumber methods, Society of Exploration Geophysics Annual General Meeting, Calgary, Alberta, Expanded Abstracts.

[44] Olowofela, J.A., Badmus, B.S., Ganiyu, S.A., Olurin, O.T., Babatunde, P. (2011): Source location and depth estimation from digitised aeromagnetic data acquired from the basement complex formation. *Earth Science India*, 4, pp. 136–142.

[45] Geosoft INC. (2010). Geosoft INC. 85 Richmond Street, 8th Floor, Toronto, Ontario, Canada.

[46] Frantisek, H., Jiri, P., Jazek, J. Chadina, M. (2009): Out – of- Phase Magnetic Susceptibility of rocks and soil rapid tool for magnetic granulometry. *Geophysical Journal International,* 194, pp. 170–181.